Unidirectional electromagnetic windmill scattering in a magnetized gyromagnetic cylinder

Jianfeng Chen (陈剑锋)[1,†], Jianbo Pan (潘剑波)[1,†], Yidong Zheng (郑义栋)[1], Wenyao Liang (梁文耀)[1], and Zhi-Yuan Li (李志远)[1,2*]

[1] School of Physics and Optoelectronics, South China University of Technology, Guangzhou 510640, China

[2] State Key Laboratory of Luminescent Materials and Devices, South China University of Technology, Guangzhou 510640, China

*Corresponding author: phzyli@scut.edu.cn

We present a discovery of an unusual unidirectionally rotating windmill scattering of electromagnetic waves by a magnetized gyromagnetic cylinder via an analytical theory for rigorous solution to fields and charges and an understanding of the underlying mathematical and physical mechanisms. Mathematically, the generation of nonzero off-diagonal components can break the symmetry of forward and backward scattering coefficients, producing unidirectional windmill scattering. Physically, this windmill scattering originates from the nonreciprocal unidirectional rotation of polarized magnetic charges on the surface of a magnetized gyromagnetic cylinder, which drives the scattering field to radiate outward in the radial direction and unidirectionally emit in the tangential direction. Interestingly, the unidirectional electromagnetic windmill scattering is insensitive to the excitation direction. Moreover, we also discuss the size dependence of unidirectional windmill scattering by calculating the scattering spectra of the gyromagnetic cylinder. These results are helpful for exploring and understanding novel interactions between electromagnetic waves and gyromagnetic materials or structures and offer deep insights for comprehending topological photonic states in gyromagnetic systems from the aspect of fundamental classical electrodynamics and electromagnetics.

Keywords: unidirectional electromagnetic windmill scattering; magnetized gyromagnetic cylinder; topological photonics.
DOI: 10.3788/COL202220.053901

1. Introduction

Scattering of light and electromagnetic waves by particles and cylinders is one of the most fundamental problems in classical electrodynamics, electromagnetics, and optics. Rayleigh made the first, to the best of our knowledge, quantitative study[1,2], and, subsequently, Mie established the rigorous scattering theory for a homogeneous sphere of arbitrary size, which was then extended to solve the infinite isotropic cylinder[3,4]. Recently, electromagnetic scattering by an anisotropic cylinder with off-diagonal permittivity and permeability tensors has attracted great attention[5–7]. On the other hand, various numerical methods have existed to solve the scattering problems of an anisotropic cylinder, such as the wave spectral method[8,9], the frequency domain finite difference method[10], the dyadic Green's function method[11], the Fourier expansion method[12], and the finite element method[13].

Gyromagnetic material, as one of the most representative anisotropic media, possesses a unique permeability tensor with antisymmetrical and imaginary off-diagonal components[14,15]. It has been widely used in optical technologies such

as self-collimation[16], optical isolation[17], nonreciprocal Goos–Hänchen shift[18], and negative refraction[19,20]. Recently, it has become an excellent platform to investigate the fundamental physics underlying topologically protected one-way edge states called the topological photonic state (TPS)[21–36], which is inspired from the analogy between photon transports in gyromagnetic photonic crystals and electron quantum Hall effects in condensed matter physics systems[37,38].

Most of the previous works rely on band theories and mathematically topological concepts to understand the existence of TPS and have achieved great successes. Nevertheless, only a few of them have explained the formation mechanism of the unique behavior of the energy vortex unidirectionally rotating and cycling around the magnetized gyromagnetic cylinder, which is the most important feature of TPS; hereafter, we call it electromagnetic windmill scattering. Generally, there is a simple thought that this originates from the time reversal symmetry breaking of the system[21–38]; however, how this general rule of physics explicitly produces the electromagnetic windmill scattering is obscure. Very recently, Chen *et al.* qualitatively
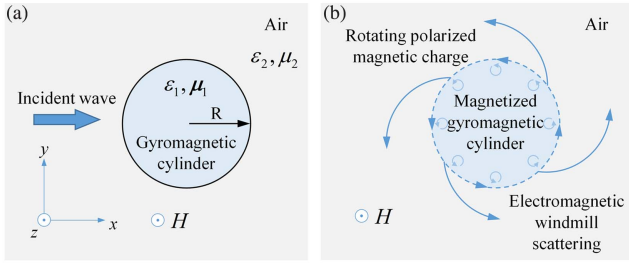
Fig. 1. Model and physics. (a) Geometry model of analytical theory. (b) Physical mechanism of electromagnetic windmill scattering.

analyzed the formation mechanism of electromagnetic windmill scattering from the aspect of instantaneous energy flow and vividly constructed the physical picture of TPS in various gyromagnetic systems[39]. It is a pity that this method cannot give the explicit solutions that enable one to quantitatively understand the physical mechanism of the interactions between the electromagnetic wave and the gyromagnetic material or structure and know how to accurately control the electromagnetic scattering by a magnetized gyromagnetic cylinder.

In this Letter, we present the rigorous solutions to the electromagnetic scattering of a magnetized gyromagnetic cylinder via analytical theory, where the model is schematically illustrated in Fig. 1(a), and uncover an unusual unidirectionally rotating windmill scattering phenomenon of electromagnetic waves. We will disclose and reveal the physical origin of this unique electromagnetic windmill scattering from well-established fundamental principles and quantities of electrodynamics and electromagnetics, as plotted in Fig. 1(b). We find that the incoming plane wave can excite unidirectionally rotating polarized magnetic charges on the boundary of the magnetized gyromagnetic cylinder (marked as the dotted arrows). As a result, the scattering field radiates outward in the radial direction and emits unidirectionally in the tangential direction (marked as the solid arrows) to form the unique electromagnetic windmill scattering. Interestingly, the unidirectional electromagnetic windmill scattering is insensitive to the excitation direction. Moreover, we also discuss the size dependence of unidirectional windmill scattering by calculating the scattering spectra of the gyromagnetic cylinder.

2. Analytical Theory

We first present the rigorous analytical solution to the electromagnetic scattering of a plane wave by the magnetized gyromagnetic cylinder. The gyromagnetic cylinder [yttrium-ion-garnet (YIG)] of radius r with relative permittivity $\varepsilon_1 = 15.26$ is embedded in air ($\varepsilon_2 = 1$ and $\mu_2 = 1$), as shown in Fig. 1. When a direct current (dc) magnetic field is applied in the out-of-plane (z-axis) direction, the permeability tensor of the magnetized gyromagnetic cylinder is of antisymmetric form as[14]

$$\boldsymbol{\mu}_1 = \begin{pmatrix} \mu_r & i\mu_\varphi & 0 \\ -i\mu_\varphi & \mu_r & 0 \\ 0 & 0 & 1 \end{pmatrix}, \qquad (1)$$

where $\mu_r = 1 + \frac{\omega_0 \omega_m}{\omega_0^2 - \omega^2}$ and $\mu_\varphi = \frac{\omega \omega_m}{\omega_0^2 - \omega^2}$. $\omega_0 = 2\pi\gamma H_0$ is the resonance frequency with $\gamma = 2.8$ MHz/Oe being the gyromagnetic ratio, and $\omega_m = 2\pi\gamma M_s$ is the characteristic circular frequency with M_s being the saturation magnetization ($M_s = 1780$ Gauss).

Without loss of generality, the time dependence of a harmonic electromagnetic wave is assumed to be $e^{-i\omega t}$. The electric and magnetic fields of the magnetized gyromagnetic cylinder satisfy the following Maxwell's equations:

$$\nabla \times \boldsymbol{H} = -i\omega\varepsilon_0\varepsilon_1\boldsymbol{E}, \qquad \nabla \times \boldsymbol{E} = i\omega\mu_0\boldsymbol{\mu}_1\boldsymbol{H}, \qquad (2)$$

where ε_0 and μ_0 are the vacuum permittivity and permeability, respectively. Generally, for most anisotropic materials, there is no symmetry with rotational and/or translational invariance, so Maxwell's equations cannot yield to generalized Helmholtz equations for electric and magnetic fields that allow one to implement separation of variables[8–13]. Yet, thanks to the special permeability tensor of the magnetized gyromagnetic cylinder possessing the antisymmetrical imaginary off-diagonal components, here, Maxwell's equations can be accurately solved.

To simplify, we only consider the transverse-electric (TE) incident wave, defined by wave vector k, with its electric field polarized along the z-axis direction, so $(E_z, H_r, H_\varphi) \neq 0$ and $(H_z, E_r, E_\varphi) = 0$. In cylindrical coordinates, the plane wave $e^{ikr\cos\varphi}$ can be expanded into the sum of a series of cylindrical waves $\sum_{n=-\infty}^{+\infty} i^n J_n(kr)e^{in\varphi}$ by the Jacobi–Anger identity, so the fields of every eigenstate have the $e^{in\varphi}$ dependence with φ being the azimuthal angle and n being the azimuthal quantum number. Notably, the positive and negative n represent the clockwise and counterclockwise rotating eigenstates, respectively.

When an incident plane wave with frequency f impinges upon the magnetized gyromagnetic cylinder, the total field can be written as the sum of the elementary incident field and the secondary scattering field arising from the polarized cylinder. The solutions of the electric field inside and outside of the cylinder can be expressed as[4]

$$E_z^{\text{in}} = \sum_{n=-\infty}^{+\infty} i^n d_n J_n(k_1 r)e^{in\varphi}, \qquad r < a, \qquad (3)$$

$$E_z^{\text{out}} = \sum_{n=-\infty}^{+\infty} i^n [J_n(k_2 r) + b_n H_n(k_2 r)]e^{in\varphi}, \qquad r > a, \qquad (4)$$

where $k_1 = k_0\sqrt{\varepsilon_1\mu_1}$, $k_2 = k_0\sqrt{\varepsilon_2\mu_2}$, with $k_0 = \omega/c = 2\pi f/c$ being the free-space wave number. The function $H_n(k_2 r)$ denotes the nth-order Hankel function of the first kind, which is chosen because of its asymptotic behavior. When combined with the factor $e^{-i\omega t}$, it represents an outgoing cylindrical wave, as is required for the secondary scattering field of the polarized cylinder. Furthermore, the tangential magnetic fields in the magnetized gyromagnetic cylinder and air are

$$H_\varphi^{in} = i\frac{1}{\omega\mu_0\mu_1}\left(\frac{\partial E_z^{in}}{\partial r} + \frac{\mu_\varphi}{\mu_r}\frac{n}{r}E_z^{in}\right), \qquad r < a, \qquad (5)$$

$$H_\varphi^{out} = i\frac{1}{\omega\mu_0\mu_2}\frac{\partial E_z^{out}}{\partial r}, \qquad r > a. \qquad (6)$$

Solving Maxwell's equations together with the boundary conditions yields the scattering coefficients given by

$$b_n = \frac{R_n(k_1a)J_n(k_2a) - k_2J_n(k_1a)J_n'(k_2a)}{k_2J_n(k_1a)H_n'(k_2a) - R_n(k_1a)H_n(k_2a)}, \qquad (7)$$

$$d_n = \frac{k_2J_n(k_2a)H_n'(k_2a) - k_2J_n'(k_2a)H_n(k_2a)}{k_2J_n(k_1a)H_n'(k_2a) - R_n(k_1a)H_n(k_2a)}, \qquad (8)$$

where $R_n(k_1a) = \frac{\mu_2}{\mu_1}[k_1J_n'(k_1a) + \frac{\mu_\varphi}{\mu_r}\frac{n}{a}J_n(k_1a)]$. The detailed derivation process can be viewed in Supplementary Materials.

3. Electromagnetic Windmill Scattering

We perform numerical calculations based on the analytical solutions on the electric field patterns of a left-incident plane wave at $f = 4.0$ GHz, illuminating the magnetized gyromagnetic cylinder. The external magnetic field is $H_0 = 1600$ Gauss. Figures 2 and 3 show the electric field distributions at different time phases for radius $R_1 = 4.20$ mm and $R_2 = 6.76$ mm, respectively, and one should note that T is the period of time phases. As shown in Fig. 2, a clear counterclockwise dipole-like radiation state is dominantly excited on the cylinder. As time elapses, the two poles with prominent tails of light, together with the whole electric field, rotate counterclockwise, leading to the two-blade windmill scattering electric field distribution (for better visual effect, see Visualization 1).

For the case of $R_2 = 6.76$ mm, Fig. 3 shows a counterclockwise quadrupole-like windmill electric field distribution unidirectionally rotating and cycling around the cylinder, also with
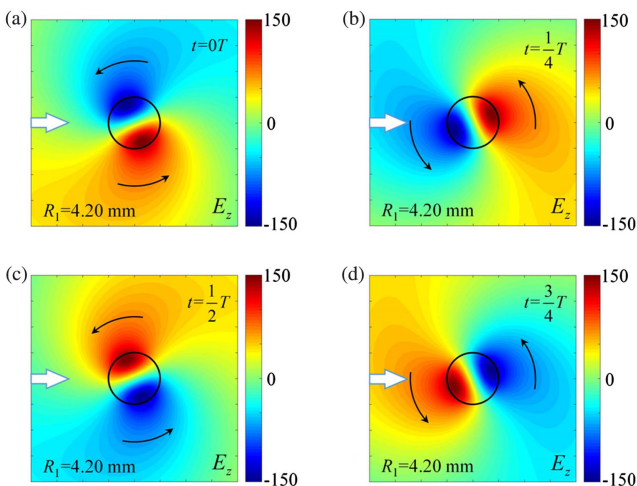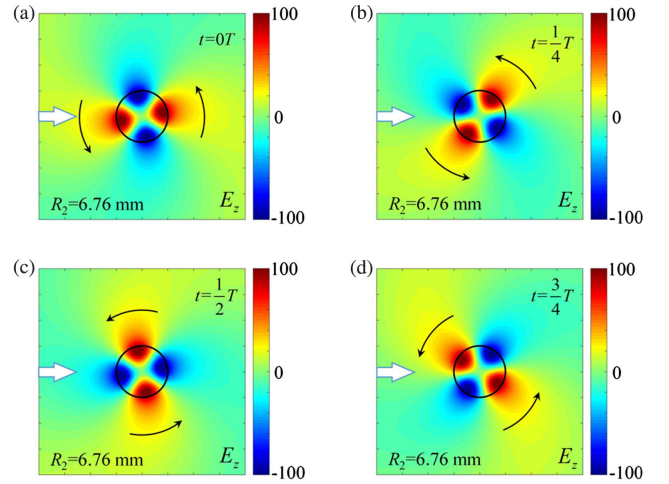

Fig. 3. Numerical calculation results of $R_2 = 6.76$ mm. (a) $t = 0T$, (b) $t = T/4$, (c) $t = T/2$, (d) $t = 3T/4$.

prominent tails of light (for better visual effect, see Visualization 2). Remarkably, these results are completely different from the well-known electric field scattering pattern observed in the nonmagnetized gyromagnetic cylinder and also have never been reported by analytical theory before. Moreover, we also calculate the scattering spectra of these two magnetized gyromagnetic cylinders at different frequencies, and the detailed results can be seen in Supplementary Materials.

We have shown the electric field distributions of the gyromagnetic cylinder at different time phases to observe the unidirectional windmill scattering. Here, we proceed to calculate the energy flux or Poynting vector $S = \frac{1}{2}\text{Re}[E \times H^*]$ distribution to exhibit the time-averaged responses in both near-field and far-field. The plane wave at $f = 4.0$ GHz is incident from the left port (marked as the thick white arrows). The energy flux and electric field distributions of $R_1 = 4.20$ mm and $R_2 = 6.76$ mm are superposed together, as shown in Figs. 4(a) and 4(b). In near-field, the majority of energy flux is concentrated on the gyromagnetic cylinder and rotates counterclockwise to form two clear counterclockwise energy flux loops, while in far-field, the prominent tails of the dipole and quadrupole exist, as seen by the thin white arrows in Fig. 4.
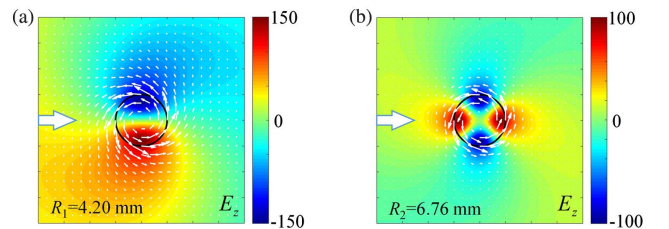

Fig. 2. Numerical calculation results of $R_1 = 4.20$ mm. (a) $t = 0T$, (b) $t = T/4$, (c) $t = T/2$, (d) $t = 3T/4$.

Fig. 4. Energy flux (Poynting vector) distribution of unidirectional windmill scattering. (a) $R_1 = 4.20$ mm, (b) $R_2 = 6.76$ mm. The thick white arrows indicate the left-incident plane wave at $f = 4.0$ GHz. The thin white arrows represent the energy flux distribution, and the directions of the thin white arrows indicate the transport direction of energy fluxes.

4. Mathematical Mechanism

Next, we analyze the mathematical mechanism of nonreciprocal unidirectional windmill scattering from the electromagnetic scattering coefficient formulae. We can see that for the magnetized gyromagnetic cylinder, the existence of a nonzero off-diagonal component ($\mu_\varphi \neq 0$) induces the appearance of a linear term related with the azimuthal quantum number n in the tangential magnetic field, as seen in Eq. (5), so that the symmetry between positive n and negative n of the tangential magnetic field is broken. This result indicates that the clockwise and counterclockwise rotating tangential magnetic fields are asymmetrical, so the propagation behaviors of the tangential magnetic field are nonreciprocal, reflecting the effect of the time reversal symmetry breaking. On the other hand, for the tangential magnetic field outside of the cylinder, since it is a nonmagnetic medium, there is no additional linear term related to n [see Eq. (6)], so the positive-n and negative-n tangential magnetic fields are symmetrical, and the propagation behaviors of the tangential magnetic fields are reciprocal.

However, the nonreciprocal propagation of the tangential magnetic field inside the magnetized gyromagnetic cylinder can be transferred to the air through the boundary conditions (i.e., E_z and H_φ are continuous at the boundary) and cause the term $R_n(k_1a)$ [possessing a linear term related to n, i.e., $\frac{\mu_2}{\mu_1}\frac{\mu_\varphi}{\mu_r}\frac{n}{a}J_n(k_1a)$] that appears in the scattering coefficients b_n and d_n. In this case, $R_n(k_1a)$ and $R_{-n}(k_1a)$ are linearly independent, so the positive and negative nth-order scattering coefficients of the electric fields are not equal (i.e., $b_n \neq b_{-n}$ and $d_n \neq d_{-n}$), indicating that the clockwise and counterclockwise scattering electric fields are asymmetrical.

Therefore, this mathematical analysis enables us to get a clear physical picture where the strong imbalance between the asymmetrical clockwise and counterclockwise rotation eigenstates forms the traveling-like wave state instead of the standing-like wave state when in the reciprocal case. In addition to radiating outward, the scattering wave will rotate and cycle around the magnetized gyromagnetic cylinder, leading to the generation of the unique unidirectional windmill scattering. This physical picture given by the mathematical analysis is completely consistent with the peculiar electric field transport characteristics as calculated by the analytical theory in Section 3. Notably, when the cylindrical coordinate transfers to the rectangular coordinate, the nonzero off-diagonal component will break the symmetry of forward and backward scattering coefficients, instead of the clockwise and counterclockwise scattering coefficients.

On the contrary, when the external magnetic field is removed, the permeability tensor reduces to scalar, i.e., $\mu_r = 1$ and $\mu_\varphi = 0$. The linear term related to n disappears, i.e., $R_n(k_1a) = k_1 J'_n(k_1a)$. In this case, $R_n(k_1a)$ and $R_{-n}(k_1a)$ are linearly dependent, and the positive and negative nth-order scattering coefficients are the same, i.e., $b_n = b_{-n}$ and $d_n = d_{-n}$. As a result, the completely balanced interference of the symmetrical clockwise and counterclockwise rotation eigenstates forms the standing-like wave state instead of the traveling-like wave state, so the scattering field only radiates outward in the radial direction without any deflection in the tangential direction. Thus, the scattering electromagnetic field will be symmetrical about the direction of the incoming plane wave, in complete consistence with the scattering field distribution around a nonmagnetic dielectric cylinder[4].

5. Physical Mechanism

Section 3 has shown the unidirectional windmill scattering calculated by analytical theoretical solutions, and this unique phenomenon is completely consistent with the clear physical picture given by mathematical analysis in Section 4, but the physical origin is still unclear. From the basic physical point of view, the macroscopic electromagnetic scattering by the medium should be the result of the interaction between the incoming electromagnetic field and the polarization charge or the magnetized current. Thus, solving the polarized magnetic charge distribution within the magnetized gyromagnetic cylinder becomes the key to revealing the microscopic physical origin of the macroscopic electromagnetic windmill scattering.

We obtain the polarized magnetic charge density via the formula $\rho_m = -\mu_0 \nabla \cdot \boldsymbol{M}$ based on simultaneous equations $\nabla \cdot \boldsymbol{B} = 0$ and $\boldsymbol{B} = \mu_0(\boldsymbol{H} + \boldsymbol{M})$, where $\boldsymbol{M}$, $\boldsymbol{B}$, and $\boldsymbol{H}$ are the magnetization, magnetic strength, and magnetic field strength, respectively[40]. The magnetization $\boldsymbol{M} = \chi_m \boldsymbol{H} = (\boldsymbol{\mu} - 1)\boldsymbol{H}$, where χ_m is the magnetic susceptibility of the medium. In the absence of an external magnetic field, $\chi_m = 0$ and $\boldsymbol{\mu} = 1$ in both the gyromagnetic cylinder and air, so their magnetizations are zero (i.e., $\boldsymbol{M}_1 = \boldsymbol{M}_2 = 0$). Instead, when the external magnetic field is applied, χ_m in air is still zero ($\boldsymbol{M}_2 = 0$), but χ_m in the magnetized gyromagnetic cylinder becomes a magnetic susceptibility tensor. For the magnetized gyromagnetic cylinder, $\boldsymbol{M}_1 \neq 0$, and we obtain

$$\boldsymbol{M}_r = \frac{1}{\omega\mu_0\mu_1}\left[(\mu_r - 1)\left(\frac{n}{r}\boldsymbol{E}_z + \frac{\mu_\varphi}{\mu_r}\frac{\partial \boldsymbol{E}_z}{\partial r}\right) - \mu_\varphi\left(\frac{\partial \boldsymbol{E}_z}{\partial r} + \frac{\mu_\varphi}{\mu_r}\frac{n}{r}\boldsymbol{E}_z\right)\right],$$
(9)

$$\boldsymbol{M}_\varphi = \frac{i}{\omega\mu_0\mu_1}\left[(\mu_r - 1)\left(\frac{\mu_\varphi}{\mu_r}\frac{n}{r}\boldsymbol{E}_z + \frac{\partial \boldsymbol{E}_z}{\partial r}\right) - \mu_\varphi\left(\frac{n}{r}\boldsymbol{E}_z + \frac{\mu_\varphi}{\mu_r}\frac{\partial \boldsymbol{E}_z}{\partial r}\right)\right],$$
(10)

$$\boldsymbol{M}_z = 0.$$
(11)

Obviously, the positive and negative nth-order $\boldsymbol{M}_r$ and $\boldsymbol{M}_\varphi$ of the magnetized gyromagnetic cylinder are not equal, so the magnetization is also asymmetrical. Then, the distribution of polarized magnetic charge density $\rho_m = -\mu_0 \nabla \cdot \boldsymbol{M}$ can be derived.

We calculate the polarized magnetic charge distributions of the magnetized gyromagnetic cylinder for $R_1 = 4.20$ mm and $R_2 = 6.76$ mm at different time phases and display the results in Figs. 5 and 6, respectively. The polarized magnetic charges are dominantly concentrated on the boundary of the cylinder, and the positive and negative of them represent the expansion and contraction of the scattering field during the rotation
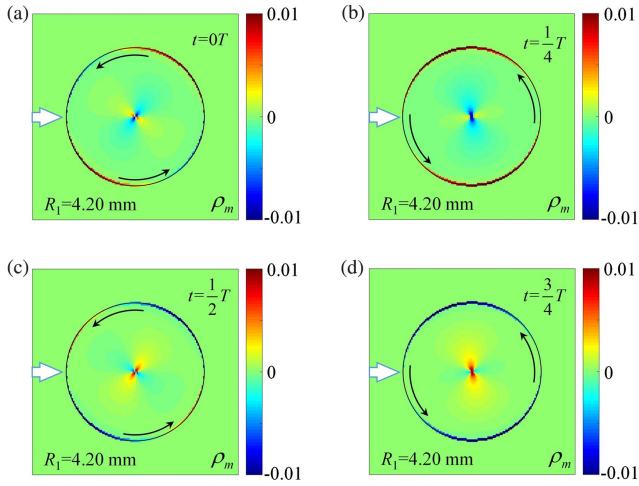
Fig. 5. Polarized magnetic charge distribution of a magnetized gyromagnetic cylinder with $R_1 = 4.20$ mm.
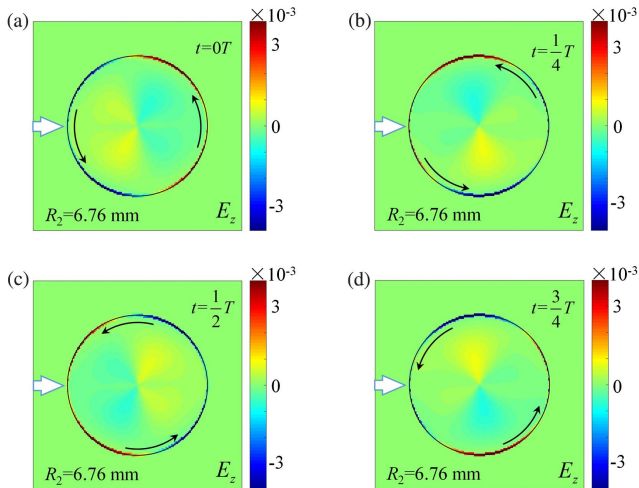

Fig. 6. Polarized magnetic charge distribution of a magnetized gyromagnetic cylinder with $R_2 = 6.76$ mm.

motion, respectively. We can see that their rotation motions are clearly visualized, which are completely consistent with the rotating and cycling windmill motion of their electric fields. For the case of $R_1 = 4.20$ mm (see Fig. 5), as time elapses, the polarized magnetic charges rotate counterclockwise along the boundary of the magnetized gyromagnetic cylinder (for better visual effect, see Visualization 3); while for the case of $R_2 = 6.76$ mm (see Fig. 6), similarly, these polarized magnetic charges also rotate counterclockwise along the boundary with time elapsing (for better visual effect, see Visualization 4). Physically, the presence of an external magnetic field breaks the time reversal symmetry of the gyromagnetic cylinder and leads to the microscopic asymmetrical response (molecular current) of the magnetized gyromagnetic cylinder. As a result, the incoming plane wave can excite the unidirectional rotation of

polarized magnetic charges on the boundary of the magnetized gyromagnetic cylinder, so the scattering field can radiate outward in the radial direction and emit unidirectionally in the tangential direction to eventually form the electromagnetic windmill scattering.

6. Scattering Properties in Various Directions

More excitingly, this unique unidirectional windmill scattering is insensitive to the excitation direction. The plane wave incident in various directions always excites the counterclockwise rotation scattering field. For example, when the right-incident and up-incident plane waves at $f = 4.0$ GHz illuminate on the magnetized gyromagnetic cylinder with $R_1 = 4.20$ mm, they both excite the dipole-like windmill scattering state that rotates counterclockwise (instead of clockwise) and only have a time phase difference in their field distribution, as shown in Figs. 7(a) and 7(b) (for better visual effect, see Visualization 5 and Visualization 6). In contrast, the scattering field of the nonmagnetic cylinder is very different from the magnetic one. We proceed to perform a numerical calculation for the dipole-like scattering of the well-studied nonmagnetized cylinder ($\varepsilon_n = 15.26$, $\mu_n = 1$, $R_0 = 5.63$ mm) at the same frequency $f = 4.0$ GHz. As shown in Figs. 7(c) and 7(d), when the right-incident and up-incident plane waves illuminate on the nonmagnetized cylinder, although they both excite the dipole-like scattering state that radiates in the fixed position, their scattering field distributions are completely distinguished. The dipole scattering fields excited by the right-incident and up-incident plane waves distribute along the x and y directions, respectively (for better visual effect, see Visualization 7 and Visualization 8). As we can see, the scattering field of the nonmagnetic cylinder is very sensitive to the excitation direction because of the absence of a unidirectional polarized magnetic charge at the interface of the nonmagnetic cylinder.
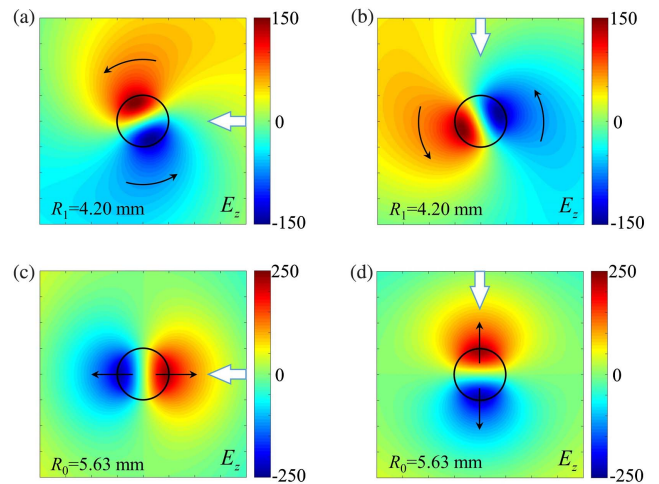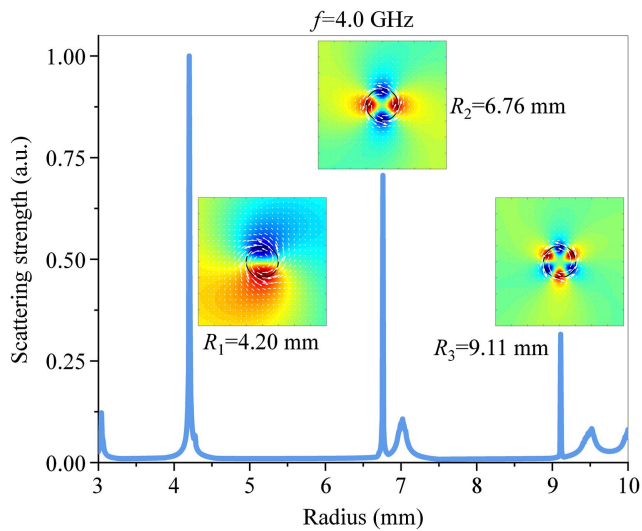

Fig. 7. Numerical calculation results of the incident plane waves in different directions. (a), (b) Magnetized gyromagnetic cylinder. (c), (d) Nonmagnetized gyromagnetic cylinder. (a), (c) Right-incident. (b), (d) Up-incident.

Fig. 8. Normalized scattering spectra varying with the radius of the magnetized gyromagnetic cylinder. Three insets indicate the electric field and energy flux distributions of R_1, R_2, and R_3.

7. Size Dependence of Unidirectional Windmill Scattering

Finally, we proceed to discuss the size dependence of unidirectional windmill scattering by calculating the normalized scattering spectra of the gyromagnetic cylinder at a radius ranging from 3.00 mm to 10.00 mm. The excited frequency of the left-incident plane wave is $f = 4.0$ GHz. As illustrated in Fig. 8, three high peaks exist at $R_1 = 4.20$ mm, $R_2 = 6.76$ mm, and $R_3 = 9.11$ mm. The electric field and energy flux distributions of these three cases are plotted as the insets of Fig. 8. One can see that there are dipole-like, quadrupole-like, and hexapole-like electric field distributions in the cases of R_1, R_2, and R_3, respectively, and this is because the excitation of these multipole states strongly enhances the scattering strength. Notably, the nonreciprocal scattering field also can be excited at other radii in the presence of the gyromagnetic effect of the magnetized gyromagnetic cylinder, but the clear counterclockwise unidirectional multipole windmill scattering only can be formed at these special radii.

8. Discussion and Conclusions

The analytical solutions of electromagnetic wave scattering by a magnetized gyromagnetic cylinder and explicit formulae on the spatial–temporal evolution of two critical physical quantities as the electromagnetic field and polarized magnetized charges enable us to comprehend the formation mechanism of unusual electromagnetic windmill scattering with prominent tails of light both in mathematics and in physics. Interestingly, this phenomenon is very similar to the windmill fireworks seen in real life. When the launcher is stationary, the fireworks only spray in the radial direction, whereas when the launcher rotates counterclockwise, the launcher will provide a tangential speed for the sprayed fireworks to produce the windmill firework emission

pattern (for better visual effect, see Visualization 9). We also provide the distributions of the windmill firework at different times in Supplementary Materials. Moreover, although we only focus on the unidirectional windmill scattering in the microwave range, these results are also suitable for other frequency ranges, even the optical range[41,42], although the gyromagnetic effect of gyromagnetic materials is quite weak at optical frequencies.

In conclusion, we have shown the rigorous explicit solutions and discovery of an unusual electromagnetic windmill scattering by a magnetized gyromagnetic cylinder. We have clarified the underlying mathematical and physical origins via analytical theory and numerical calculation and found that the unbalanced scattering coefficients for the same-order clockwise and counterclockwise cylindrical waves and unidirectionally rotating and cycling polarized magnetic charges along the air-cylinder boundary are the critical physical entities governing the observed unique nonreciprocal windmill scattering of the electromagnetic wave and field. Our results will have great significance not only in basic electrodynamics, electromagnetics, and topological photonics, but also in novel design of photonic devices[43,44].

†These authors contributed equally to this work.

References

1. L. Rayleigh, "On the light from the sky, its polarization and color," Philos. Mag. **41**, 107 (1871).
2. L. Rayleigh, "On the transmission of light through an atmosphere containing small particles in suspension and on the origin of the blue of the sky," Philos. Mag. **47**, 375 (1899).
3. M. Kerker, *The Scattering of the Light and Other Electromagnetic Radiation* (Academic, 1969).
4. H. C. V. D. Hulst, *Light Scattering by Small Particles* (Dover, 2000).
5. J. Jin, S. Liu, Z. Lin, and S. T. Chui, "Effective-medium theory for anisotropic magnetic metamaterials," Phys. Rev. B **80**, 115101 (2009).
6. J. Wang, K. H. Fung, H. Y. Dong, and N. X. Fang, "Zeeman splitting of photonic angular momentum states in a gyromagnetic cylinder," Phys. Rev. B **84**, 235122 (2011).
7. B. A. V. Tiggelen and G. L. J. A. Rikken, "Photon Hall pinwheel radiation of angular momentum by a diffusing magneto-optical medium," Phys. Rev. Lett. **125**, 133901 (2020).
8. J. C. Monzon and N. J. Damaskos, "Two-dimensional scattering by a homogeneous anisotropic rod," IEEE Trans. Antennas Propag. **34**, 1243 (1986).
9. J. C. Monzon, "Three-dimensional scattering by an infinite homogeneous anisotropic circular cylinder: a spectral approach," IEEE Trans. Antennas Propag. **35**, 670 (1987).
10. C. M. Rappaport and B. J. McCartin, "FDFD analysis of electromagnetic scattering in anisotropic media using unconstrained triangular meshes," IEEE Trans. Antennas Propag. **39**, 345 (1991).

11. F. Olyslager, "Time-harmonic two- and three-dimensional Green's dyadic for general uniaxial bianisotropic media," IEEE Trans. Antennas Propag. **43**, 430 (1995).

12. X. B. Wu and K. Yasumoto, "Cylindrical vector-wave-function representations of fields in a biaxial Ω-medium," J. Electromagn. Waves Appl. **11**, 1407 (1997).

13. R. D. Graglia and P. L. E. Uslenghi, "Electromagnetic scattering from anisotropic materials, part II: computer code and numerical results in two dimensions," IEEE Trans. Antennas Propag. **35**, 225 (1987).

14. D. M. Polaz, *Microwave Engineering* (Wiley, 1998).

15. J. Chen, W. Liang, and Z. Y. Li, "Progress of topological photonic state in magneto-optical photonic crystal," Acta Opt. Sin. **41**, 0823005 (2021).

16. Q. B. Li, Z. Li, and R. X. Wu, "Bending self-collimated one-way light by using gyromagnetic photonic crystals," Appl. Phys. Lett. **107**, 241907 (2015).

17. W. Tong, J. Wang, J. Wang, Z. Liu, Y. Pang, and S. Qu, "Magnetically tunable unidirectional waveguide based on magnetic photonic crystals," Appl. Phys. Lett. **109**, 053502 (2016).

18. H. Ma, C. Ju, X. Xi, and R. X. Wu, "Nonreciprocal Goos–Hänchen shift by topological edge states of a magnetic photonic crystal," Opt. Express, **28**, 19916 (2020).

19. C. Ju, R.-X. Wu, Z. Li, Y. Poo, S.-Y. Liu, and Z.-F. Lin, "Manipulating electromagnetic wave propagating non-reciprocally by a chain of ferrite rods," Opt. Express **25**, 22096 (2017).

20. T.-J. Guo, T.-F. Li, M. Yang, H.-X. Cui, Q.-H. Guo, X.-W. Cao, and J. Chen, "Nonreciprocal optical diffraction by a single layer of gyromagnetic cylinders," Opt. Express **22**, 537 (2014).

21. G. Harari, M. A. Bandres, Y. Lumer, M. C. Rechtsman, Y. D. Chong, M. Khajavikhan, D. N. Christodoulides, and M. Segev, "Topological insulator laser: theory," Science **359**, eaar4003 (2018).

22. M. A. Bandres, S. Wittek, G. Harari, M. Parto, J. Ren, M. Segev, D. N. Christodoulides, and M. Khajavikhan, "Topological insulator laser: experiments," Science **359**, eaar4005 (2018).

23. J. Chen, W. Liang, and Z. Y. Li, "Strong coupling of topological edge states enabling group-dispersionless slow light in magneto-optical photonic crystals," Phys. Rev. B **99**, 014103 (2019).

24. J. Chen, W. Liang, and Z. Y. Li, "Switchable slow light rainbow trapping and releasing in strongly coupling topological photonic systems," Photonics Res. **7**, 1075 (2019).

25. J. Chen, W. Liang, and Z. Y. Li, "Broadband dispersionless topological slowlight," Opt. Lett. **45**, 4964 (2020).

26. T. Lin, Z. Chen, X. Zhang, H. Li, X. Liu, and H. Lü, "Experimental observation of topologically protected defect states in silicon waveguide arrays," Chin. Opt. Lett. **18**, 051301 (2020).

27. L. Chen, R. K. Singh, A. Dogariu, Z. Chen, and J. Pu, "Estimating topological charge of propagating vortex from single-shot non-imaged speckle," Chin. Opt. Lett. **19**, 022603 (2021).

28. L. Lu, H. Gao, and Z. Wang, "Topological one-way fiber of second Chern number," Nat. Commun. **9**, 5384 (2018).

29. Z. Wang, Y. D. Chong, J. D. Joannopoulos, and M. Soljačić, "Reflection-free one-way edge modes in a gyromagnetic photonic crystal," Phys. Rev. Lett. **100**, 013905 (2008).

30. Z. Wang, Y. D. Chong, J. D. Joannopoulos, and M. Soljačić, "Observation of unidirectional backscattering-immune topological electromagnetic states," Nature **461**, 772 (2009).

31. H. Liu, B. Xie, H. Cheng, J. Tian, and S. Chen, "Topological photonic states in artificial microstructures," Chin. Opt. Lett. **19**, 052602 (2021).

32. J. X. Fu, R. J. Liu, and Z. Y. Li, "Robust one-way modes in gyromagnetic photonic crystal waveguides with different interfaces," Appl. Phys. Lett. **97**, 041112 (2010).

33. Y. Poo, R. X. Wu, Z. F. Lin, Y. Yang, and C. T. Chan, "Experimental realization of self-guiding unidirectional electromagnetic edge states," Phys. Rev. Lett. **106**, 093903 (2011).

34. J. Chen, W. Liang, and Z. Y. Li, "Antichiral one-way edge states in a gyromagnetic photonic crystal," Phys. Rev. B **101**, 214102 (2020).

35. P. Zhou, G. G. Liu, Y. Yang, Y. H. Hu, S. Ma, H. Xue, Q. Wang, L. Deng, and B. Zhang, "Observation of photonic antichiral edge states," Phys. Rev. Lett. **125**, 263603 (2020).

36. F. F. Li, H. X. Wang, Z. Xiong, Q. Lou, P. Chen, R. X. Wu, Y. Poo, J. H. Jiang, and S. John, "Topological light-trapping on a dislocation," Nat. Commun. **9**, 2462 (2018).

37. S. Raghu and F. D. M. Haldane, "Analogs of quantum-Hall-effect edge states in photonic crystals," Phys. Rev. A **78**, 033834 (2008).

38. F. D. M. Haldane and S. Raghu, "Possible realization of directional optical waveguides in photonic crystals with broken time-reversal symmetry," Phys. Rev. Lett. **100**, 013904 (2008).

39. J. Chen, W. Liang, and Z. Y. Li, "Revealing photonic Lorentz force as the microscopic origin of topological photonic states," Nanophotonics **9**, 3217 (2020).

40. J. D. Jackson, *Classical Electrodynamics*, 3rd ed. (Wiley, 1998).

41. B. Bahari, A. Ndao, F. Vallini, A. E. Amili, Y. Fainman, and B. Kanté, "Nonreciprocal lasing in topological cavities of arbitrary geometries," Science **358**, 636 (2017).

42. B. Bahari, L. Hsu, S.-H. Pan, D. Preece, A. Ndao, A. E. Amili, Y. Fainman, and B. Kanté, "Photonic quantum Hall effect and multiplexed light sources of large orbital angular momenta," Nat. Phys. **17**, 700 (2021).

43. D. Wang, X. Jin, J. Zhao, Y. Wang, L. Rong, and J. J. Healy, "Continuous-wave terahertz diffraction tomography for measuring three-dimensional refractive index maps," Chin. Opt. Lett. **19**, 123701 (2021).

44. Y. Zhao, Q. Huang, H. Cai, X. Lin, H. He, H. Cheng, and Y. Lu, "Ultrafast control of slow light in THz electromagnetically induced transparency metasurfaces," Chin. Opt. Lett. **19**, 073602 (2021).